Negative Ion Volume Production in ECR Hydrogen Plasmas

Osamu Fukumasa and Masanori Matsumori

Department of Electrical and Electronic Engineering,

Faculty of Engineering, Yamaguchi University,

2-16-1 Tokiwadai, Ube 755-8611, Japan

Abstract

Production and control of electron cyclotron resonance(ECR) plasmas for negative ion sources have been studied. A new production method using permanent magnets is proposed as one possibility for a large diameter high density uniform microwave plasma. The microwave power is launched by an annular slot antenna into the circumference of a chamber with a ring-cusp type or a line-cusp type permanent magnets, where magnetic field can be applied in the local region and plasmas can be efficiently generated if the ECR condition is satisfied. In this paper, we report the structure of the ECR negative ion source, the characteristics of the ECR plasmas, and comparison of the ECR plasmas with DC discharge plasmas from a viewpoint of negative ion source.

KEYWORDS : negative ion source, NBI heating, ECR plasma, H^- production, magnetic filter

1. Introduction

In a design of a neutral beam injection (NBI) system for future large fusion experimental devices, such as International Thermonuclear Experimental Reactor (ITER), a deuterium negative ion source with an energy of several hundreds keV is proposed to be used. In the present positive ion sources for the NBI system, the source plasma is generated by DC arc discharge with a hot filament as a cathode, as well as in the negative ion sources under development. Lifetime of the ion source is limited to several hundred hours due to erosion and fatigue of the cathode-filaments and damage of the filaments by the anomalous arc discharge. Contamination of the plasma source by the evaporated filament materials could be also a problem in the cesium-seeded operation in the negative ion source. Besides these, in the future fusion reactor, the device materials are radio-activated due to irradiation of the neutrons yielded by the fusion reaction, and accessibility to the device is extremely limited. Thus, a long lifetime ion source is required for the future NBI system. A microwave-discharge ion source[1] and an RF-driven ion source [2,3] are promising for the long lifetime ion source, because these sources have no filaments.

In the present work, a new production method using permanent magnets is proposed as one possibility for a large diameter high density uniform microwave plasma. The microwave power is launched into the circumference of a chamber by an annular slot antenna[4] and the magnetic field of both ring-cusp type[4] and line-cusp type [5] permanent magnets. Advantages of using permanent magnets are that the magnetic field can be applied in the local region, where plasmas can be efficiently generated if the electron cyclotron resonance (ECR) condition is satisfied, and that an almost magnetic field free condition can be achieved on the extraction grid.

In this paper, we report the structure of the ECR discharge negative ion source, the characteristics of the ECR plasmas, and the optimization of the plasma parameters in the extraction region. Comparison of ECR plasmas with DC discharge plasmas from a viewpoint of the magnetic filter effect and the results of the negative ion extraction are also discussed briefly.

2. Concept of the ECR Plasma Source

A schematic diagram of the ECR hydrogen negative ion source is shown in Fig.1. The plasma source chamber (210 mm in diameter and 300 mm in length) made of stainless steel is a conventional multicusp volume source equipped with both a magnetic filter (set at z = 20 cm) and a plasma grid (set at z = 22 cm).

We test the two types of the magnetic field structure for the ECR field.

The Case I : The microwave power (2.45 GHz, 100~600 W) is transferred to the annular slot antenna[4] through a coaxial waveguide, and the microwave is launched from the antenna into the circumference of the cylindrical vacuum chamber (210 mm in diameter and 50 mm in length) through a fused silica plate window (30 mm in thickness). The width of the annular slot is 20 mm (the outer and the inner diameters are 200 and 160 mm, respectively). The ring-cusp type samarium-cobalt permanent magnets are located just outside the chamber with facing north and south polarities to the radial direction at a separation of 4 mm, as shown in Fig.1. These permanent magnets provide the resonance magnetic flux density 875 G for 2.45 GHz inside the chamber, i.e., the annular region 15 mm inside from the chamber wall.

The Case II : The microwave circuit system is the same as one for the Case I . The microwave power is launched directly into the source chamber through the fused silica plate window as shown in Fig.2. Twelve columns of samarium-cobalt permanent magnets are located just outside the source chamber. In this case, the line-cusp of permanent magnets provides both the resonance magnetic flux density 875 G for 2.45 GHz inside the chamber (i.e., the annular region 15 mm inside from the chamber wall) and confinement of the produced plasmas.

In both cases, plasma parameters are measured by two Langmuir probes movable in axial and radial directions. The right end plate, i.e. the plasma grid, has a single hole (5 mm diameter) through which negative ions were extracted from the source. A Faraday cup with separation magnet was used for measurement of the extracted H^- current.

3. Experimental Results and Discussion

3.1 DC Plasma Operation

At first, we show the characteristics of the source plasma produced by DC discharge. To this end, instead of the microwave launcher, the resonance magnet and the silica window in Figs.1 and 2, the filament flange is set in the source chamber as shown in Fig.3.

H^- ions are generated by the dissociative attachment of slow plasma electrons ($T_e \sim$ 1eV) to highly vibrationally excited hydrogen molecules, $H_2(v'' \geqq 5\text{-}6)$, where these $H_2(v'')$ are primarily produced by the collisional excitation of fast electrons with energies in excess of 20-30 eV [6,7]. Usually, this H^- production is called as the two-step volume production. With the use of the magnetic filter, the electron energy distribution is optimized for the above mentioned two-step process of H^- formation.

Figure 4 shows the typical example of spatial distributions of the plasma parameters (electron density n_e and electron temperature T_e). Because of the magnetic filter effect (M.F. is the position of the magnetic filter)[8-10], plasma parameters in the downstream region (i.e. H^- production region) is changed markedly compared with ones in the upstream region (i.e. source region or production region of highly vibrationally excited hydrogen molecules $H_2(v'')$). Namely, T_e in the downstream region is kept nearly constant although T_e in the source region increases with discharge power.

With the use of magnetic filter and the plasma grid, plasma parameters are well controlled for enhancing the two-step H^- volume production and the extraction of H^- ions. In Fig.5, for reference, we show the extracted H^- current as a function of discharge power, where discharge voltage V_d is kept constant at 80 V and discharge current I_d is varied. With increasing discharge power, extracted H^- current increases linearly.

3.2 ECR Plasmas

(1) The Case I

On production of ECR plasmas for the Case I, we reported some results elsewhere[11,12]. With

increasing microwave power $P\mu$, both n_e and T_e increase. $P\mu$ is estimated by (P_f-P_r), where P_f is the power of forward wave and P_r is the power of reflected wave. With increasing hydrogen gas pressure p, n_e increases and T_e decreases. These features of plasma parameters are nearly the same as ones in DC plasmas expect that n_e in ECR plasmas is much lower than one in DC plasmas.

Next, we discuss the axial distribution of plasma parameters (n_e and T_e), i.e. effect of magnetic filter. Figure 6 shows the typical example of axial distributions of n_e and T_e. For reference, n_e and T_e in DC plasmas are also plotted by closed circles. Here, the position of the ring-cusp type permanent magnets for ECR is set at z = -5 cm (△) and z = -1cm (□). In the resonance region, T_e is high and decreases markedly along the axial direction. In the source region (z = 0∼20), T_e keeps nearly constant value. As is shown clearly, however, T_e does not decrease or change markedly across the magnetic filter as T_e does in DC plasmas. Namely, T_e in the extraction region is rather high. Therefore, the two-step process of H^- production is not well controlled compared with the results in DC plasmas, and then the extracted H^- current is also very small.

(2) The Case II

With increasing Pμ, both n_e and T_e increase. With increasing p, n_e increases and T_e decreases. These features of plasma parameters including its value are nearly the same as ones in the Case I. However, the axial distribution of n_e and T_e is rather different from the Case I as shown in Fig.7. Particularly, T_e in the source region is higher than one in the Case I, and T_e is decreased across the magnetic filter although the value of T_e is not necessarily optimized for H^- volume production.

Next, we discuss the H^- production in the present ECR plasmas. Figure 8 shows the plasma parameters (n_e and T_e) in the first chamber (the source region) and in the second chamber (the extraction region), as a function of Pμ. They are measured at z = 15 cm in the source region and z = 21 cm in the extraction region, where the plasma grid is set at z = 22 cm. As is shown clearly, T_e in the second chamber is kept nearly constant value regardless of Pμ although the value of T_e is not

necessarily optimized for the two-step process of H^- production. On the other hand, T_e in the first chamber increases with $P\mu$.

In the present case, H^- ions are more successfully produced than ones in the Case I. Figure 9 shows the dependence of negative ion currents (i.e., H^- currents) on $P\mu$. Gas pressure p = 3 mTorr and extraction voltage Vex = 600 V. The H^- currents increase linearly with $P\mu$. According to the results shown in Fig.8, for H^- production, T_e and n_e in the second chamber are not controlled well with the magnetic filter. Besides, plasma production efficiency and also production of fast electrons are not necessarily good compared with DC plasma production. Therefore, optimization of plasma parameters for H^- production is under study and then it is also expected to enhance the H^- production in ECR plasmas.

(3) Plasma production and control of plasma parameters

On plasma production (i.e. values of n_e and T_e, pressure and $P\mu$ dependences of n_e and T_e), the Case I has nearly the same characteristics as the Case II does. However, for H^- production, plasma parameters in the Case II is more optimized. Key parameters for H^- production are fast electrons, $H_2(v'')$ and T_e. Therefore, to optimize production of fast electrons and then $H_2(v'')$, permanent magnet arrangements and antenna locations are quite important [5,13].

The role of the magnetic filter (i.e. preferential reflection of high-energy electrons) is not well clarified although it is widely used to reduce T_e. Concerning the preferential reflection of high-energy electrons, only one explanation due to velocity dependent diffusion caused by Coulomb collisions was reported[14]. A part of experimental results in high density plasmas may be explained by this model. However, magnetic filter effect is observed clearly not only in high density plasmas but also in low density (weakly ionized) plasmas[8,9]. Therefore, we proposed previously the following model[8,9] for the preferential reflection of high-energy electrons. Electrons entering the magnetic filter are trapped in filter field $\boldsymbol{B}$. Then, most electrons cross the magnetic filter due to $\boldsymbol{E} \times \boldsymbol{B}$ drift where $\boldsymbol{E}$ represents thermally excited low frequency electrostatic fluctuations. Therefore, $\boldsymbol{E} \times \boldsymbol{B}$ drift for electrons

decreases with the increase of electron velocity (i.e., energy), since fluctuating electric fields are averaged over their finite Larmor radii. Namely, high-energy electrons diffuse at a lower rate than do low-energy electrons. In the different experiment [8], plasma fluctuations with a well-defined frequency (i.e. 1-2MHz, a frequency range of lower hybrid waves) were observed. Fluctuation fields are also localized near the magnetic filter. This supports the physical picture of the magnetic filter described above.

In the proposed model described above, fluctuating field $\boldsymbol{E}$ plays an important role and $\boldsymbol{E}$ in DC plasmas should be different from that in ECR plasmas. Then, our model can be responsible for the difference of magnetic filter effect in controlling plasma parameters between DC plasmas and ECR plasmas. This point is now under study.

4. Conclusions

We have newly designed the ECR plasma source for NBI system. ECR hydrogen plasmas are well produced although n_e is lower than one in DC plasmas. We have confirmed that H^- volume production in ECR plasmas is obtained, and that effect of magnetic filter is different from one in DC plasmas. In the future, production of high density ECR plasma, optimization of plasma parameters for H^- volume production, clarifying the effect of magnetic filter and extraction of H^- ions will be studied.

Acknowledgments

The authors would like to thank Profs. T.Kuroda, O.Kaneko and Y.Takeiri, the National Institute for Fusion Science (NIFS) of Japan, and Prof. H.Fujita, Saga University, for their discussion and encouragement.

This work was supported by a Grant-in-Aid for Scientific Research from the Japanese Ministry of Education, Science, Sports and Culture. This work was also carried out as a collaboration research of the NIFS.

References

1) K. Hashimoto and S. Asano : Fusion Engineering and Design **26** (1995) 495 .

2) Y. Takeiri, T. Takanashi, O. Kaneko, Y. Oka, A. Ando, K. Tsumori and T. Kuroda : Fusion Engineering and Design **26** (1995) 501.

3) T. Takanashi, Y. Takeiri, O. Kaneko, Y. Oka, K. Tsumori and T. Kuroda : Rev. Sci. Instrum. **67** (1996) 1024.

4) T. Ikushima, Y. Okuno and H. Fujita : Appl. Phys. Lett. **64** (1994) 25.

5) O. Fukumasa, R. Itatani and S. Saeki : J. Phys. **D 18** (1985) 2433.

6) O. Fukumasa : J. Phys. **D 22** (1989) 1668.

7) O. Fukumasa : J. Appl. Phys. **71** (1992) 3193.

8) O. Fukumasa, H. Naitou and S. Sakiyama : Trans. IEE Jpn. **111A** (1991) 1057.

9) O. Fukumasa, H. Naitou and S. Sakiyama : J. Appl. Phys. **74** (1993) 848.

10) O. Fukumasa, Y. Tauchi and S. Sakiyama : Jpn. J. Appl. Phys. **36** (1997) 4593.

11) O. Fukumasa and N. Tsuda : *Proc. 8th Int.Symp. on the Production and Neutralization of Negative Ions and Beams* (Giens, 1997), p.165.

12) O. Fukumasa and M. Matsumori : The Korea-Japan Joint Workshop on Plasma Technologies and Applications (October 9-10, 1998), EP-98-75.

13) T. Namura, I. Arikata, O. Fukumasa, M. Kubo and R. Itatani : Rev. Sci. Instrum. **63** (1992) 21.

14) A. J. T. Holmes : Rev. Sci. Instrum. **53** (1982) 1517.

Figure Captions

Fig.1. Schematic diagram of the ECR negative ion source with the ring-cusp type resonance magnet.

Fig.2. Schematic diagram of the ECR negative ion source with the line-cusp type resonance magnet.

Fig.3. Schematic diagram of the DC negative ion source.

Fig.4. Axial distribution of plasma parameters in DC discharge plasmas : (a) electron density ne , (b) electron temperature Te. Experimental conditions are as follows : discharge voltage Vd = 80V, discharge current Id = 2A(●), 2.5A(○) and 3A(□), and hydrogen gas pressure $p(H_2)$ = 2mTorr. M.F. is the position of the magnetic filter. Extraction grid is set at z = 22 cm.

Fig.5. Extracted H^- current as a function of DC discharge power. Experimental conditions are as follows: Vd = 80V, $p(H_2)$ = 2mTorr, extraction voltage Vex = 600V, and Id is varied from 1 to 4A. In this experiment, the plasma grid has a single hole with 10 mm diameter, different from the case for ECR plasma experiment (5 mm diameter).

Fig.6. Axial distribution of plasma parameters in DC discharge plasma and ECR discharge plasma (Case Ⅰ): (a) ne , (b)Te . Plasma parameters of DC plasma are the same as ones (Id = 3A) in Fig.4. In ECR plasma case, $P\mu$ = 450W and $p(H_2)$ = 2mTorr.

Fig.7. Axial distribution of plasma parameters in ECR discharge plasma (Case Ⅱ) : (a) ne , (b)Te . Microwave input power $P\mu$ = 450W and $p(H_2)$ = 3.8mTorr.

Fig.8. Plasma parameters in ECR plasmas (Case Ⅱ) as a function of microwave power P_{μ} : (a)ne, (b)Te. Parameters in the source region (filled symbols) and those in the extraction region (open symbols) are measured at z = 15 cm and 21 cm, respectively. $p(H_2)$ = 3 mTorr.

Fig.9. Extracted H^-currents, corresponding to the plasma parameters in Fig.8, versus P_{μ}. Extraction voltage Vex = 600 V.

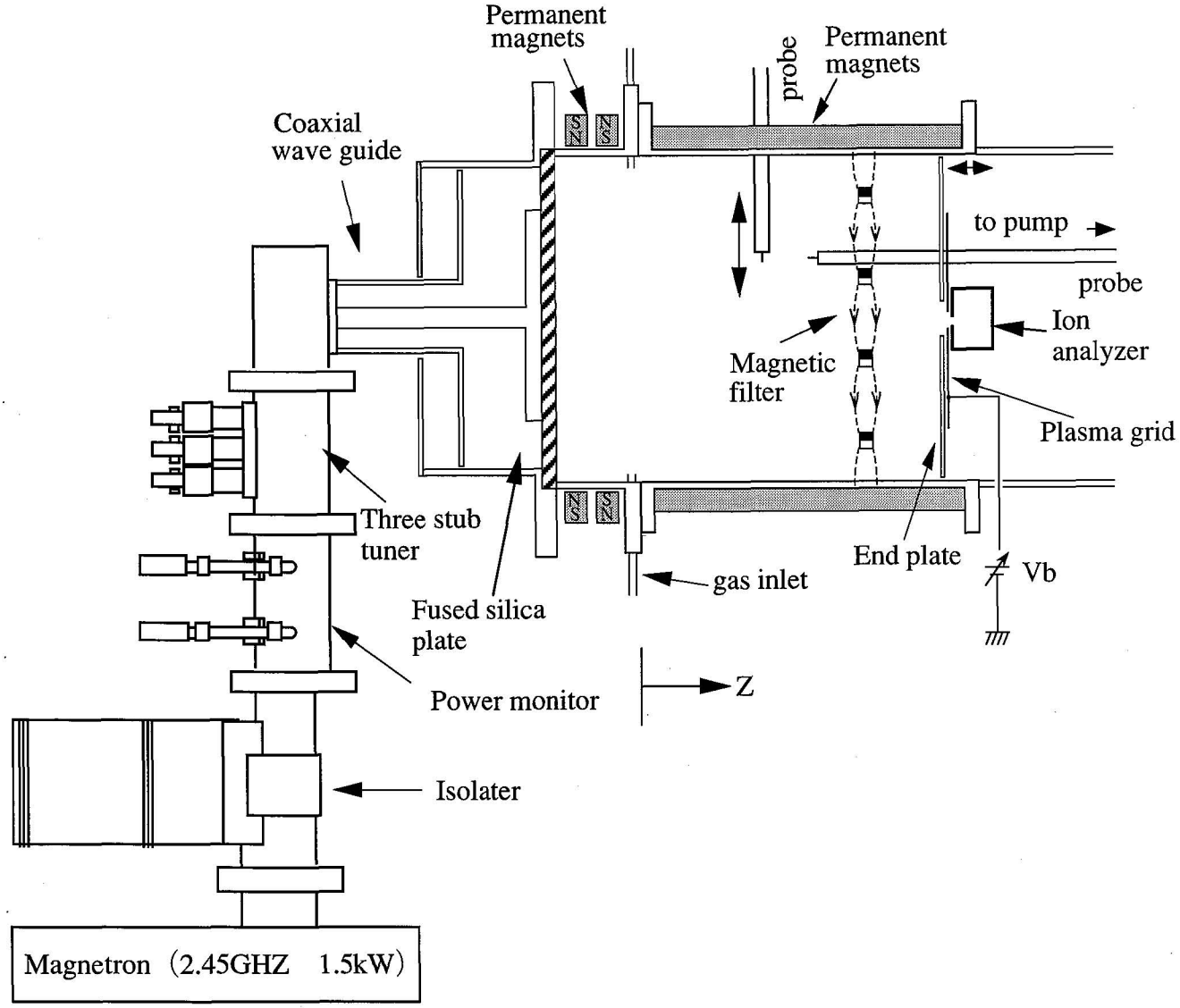
Permanent magnets
probe
Permanent magnets
Coaxial wave guide
to pump
probe
Ion analyzer
Magnetic filter
Plasma grid
Three stub tuner
Fused silica plate
gas inlet
End plate
Vb
Power monitor
Z
Isolater
Magnetron (2.45GHZ 1.5kW)

Fig.1

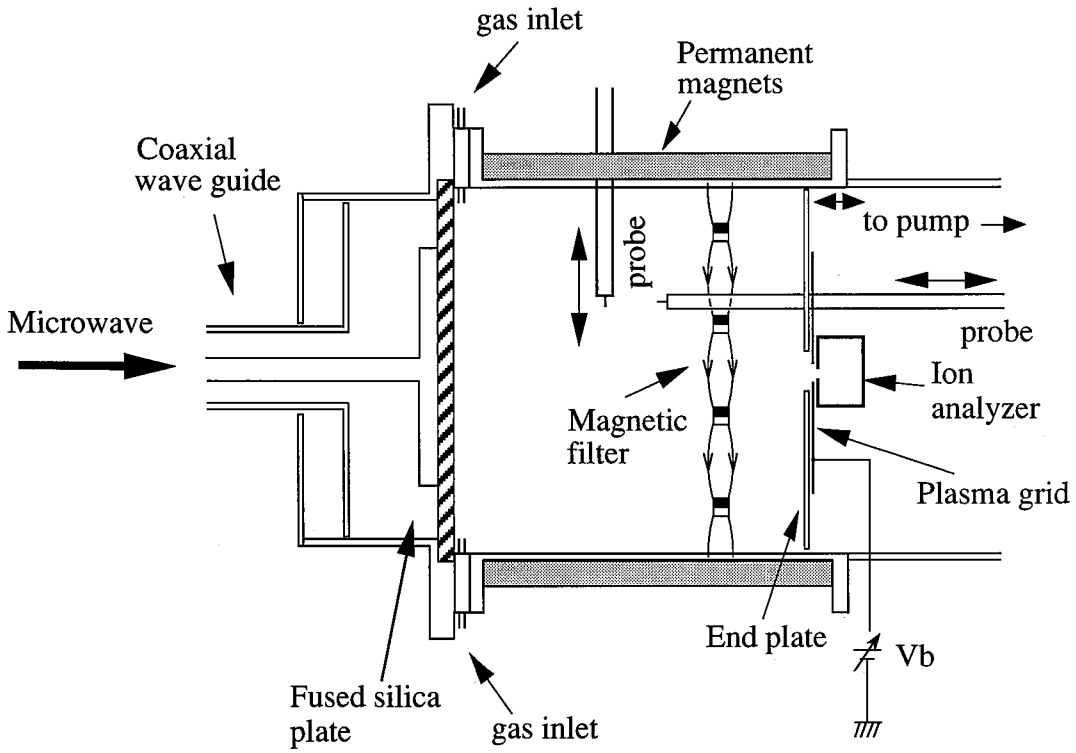
gas inlet
Permanent magnets
Coaxial wave guide
to pump
probe
Microwave
probe
Ion analyzer
Magnetic filter
Plasma grid
End plate
Vb
Fused silica plate
gas inlet

Fig.2

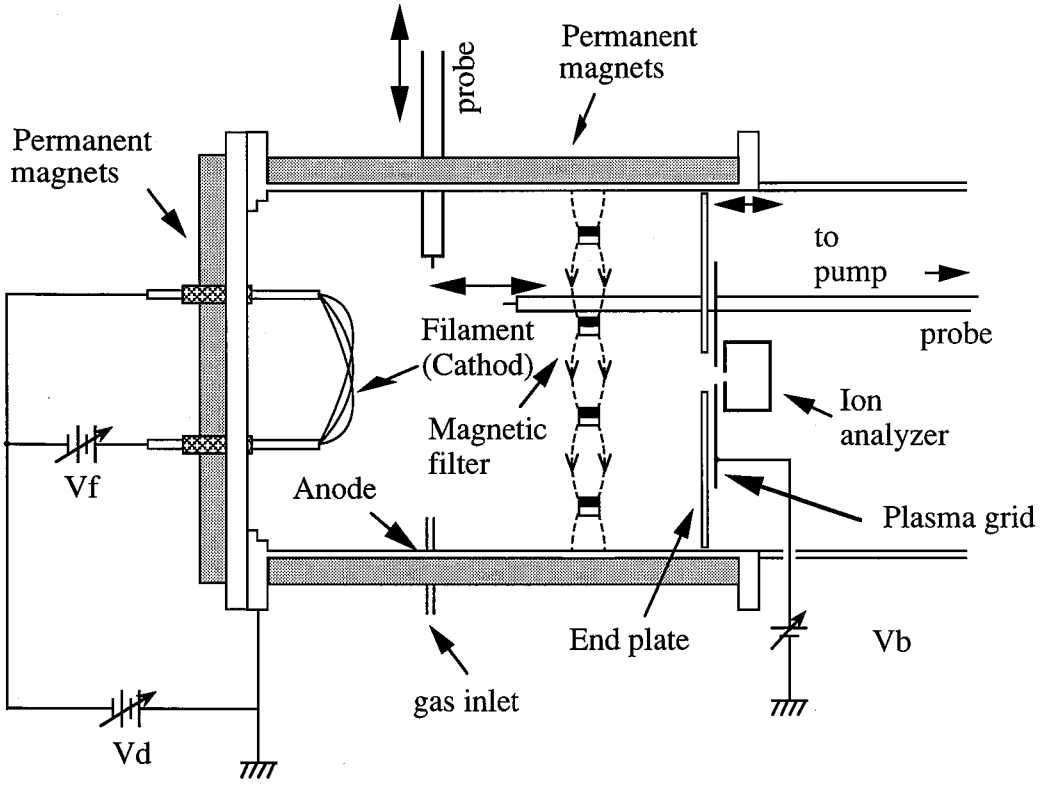
probe
Permanent magnets
Permanent magnets
to pump
probe
Filament (Cathod)
Magnetic filter
Ion analyzer
Vf
Anode
Plasma grid
End plate
Vb
gas inlet
Vd

Fig.3

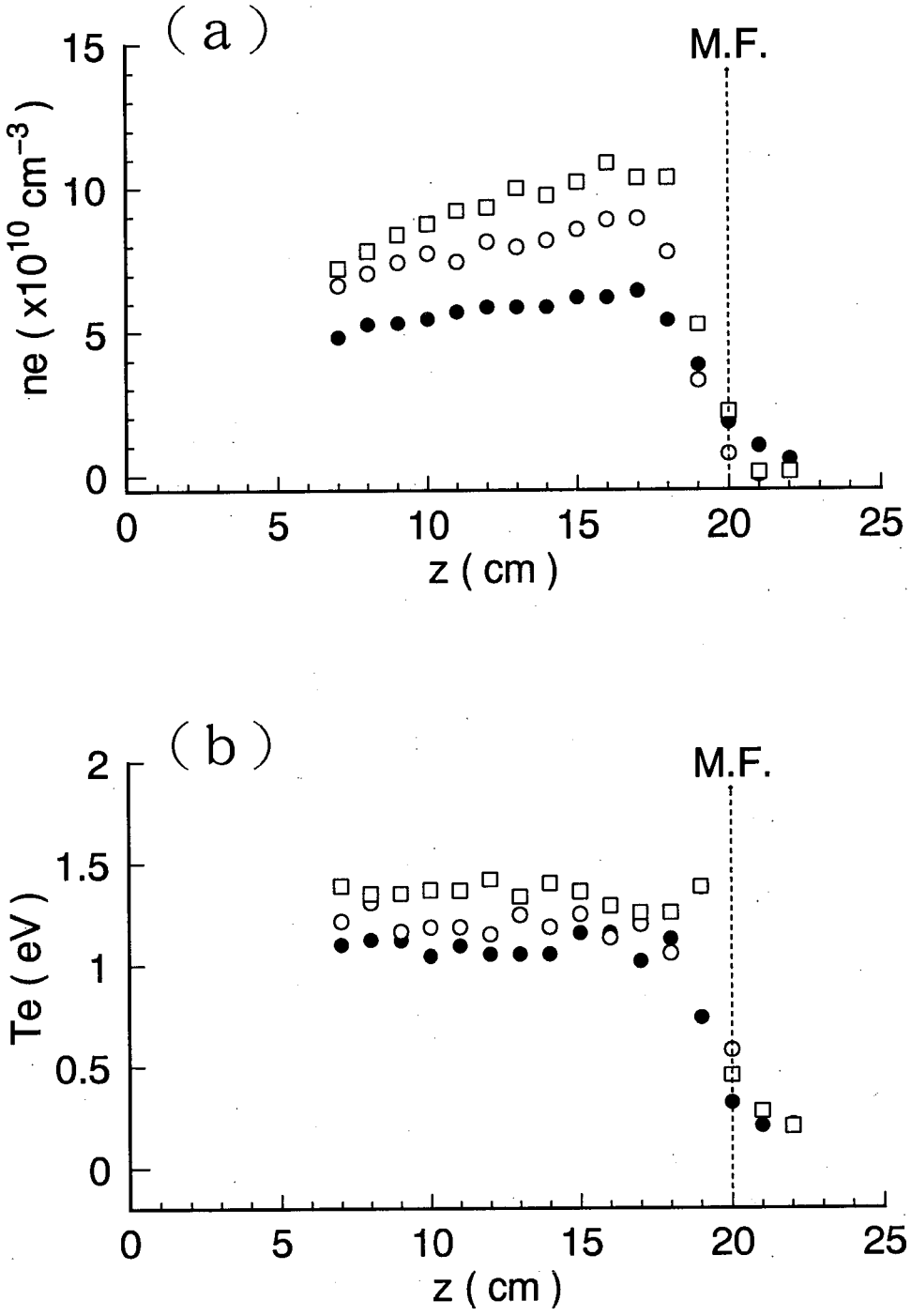
(a)
M.F.
15
10
5
0
ne (x10^10 cm^-3)
0
5
10
15
20
25
z (cm)
(b)
M.F.
2
1.5
1
0.5
0
Te (eV)
0
5
10
15
20
25
z (cm)

Fig.4

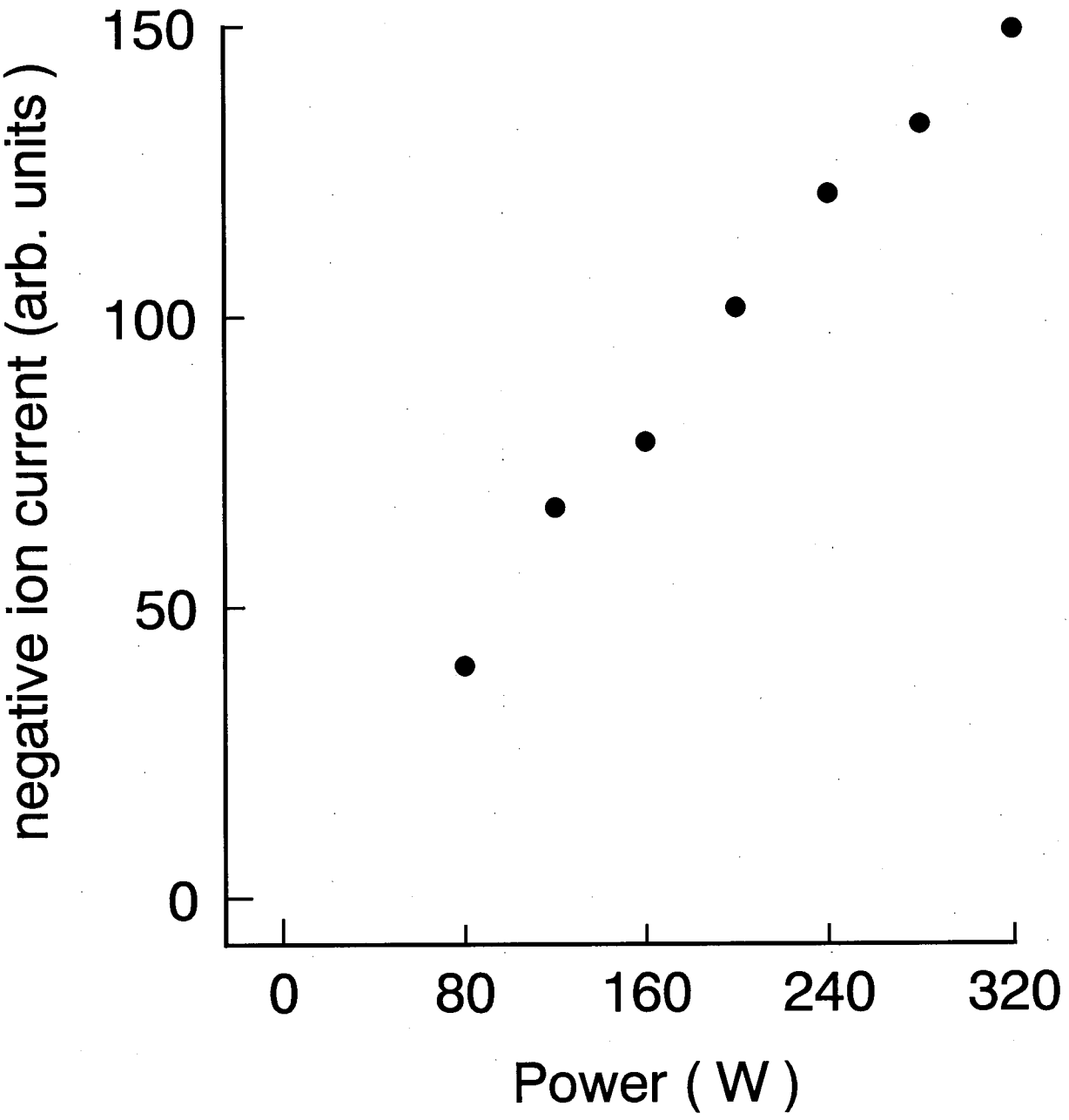
150
100
50
0
negative ion current (arb. units)
0
80
160
240
320
Power (W)

Fig.5

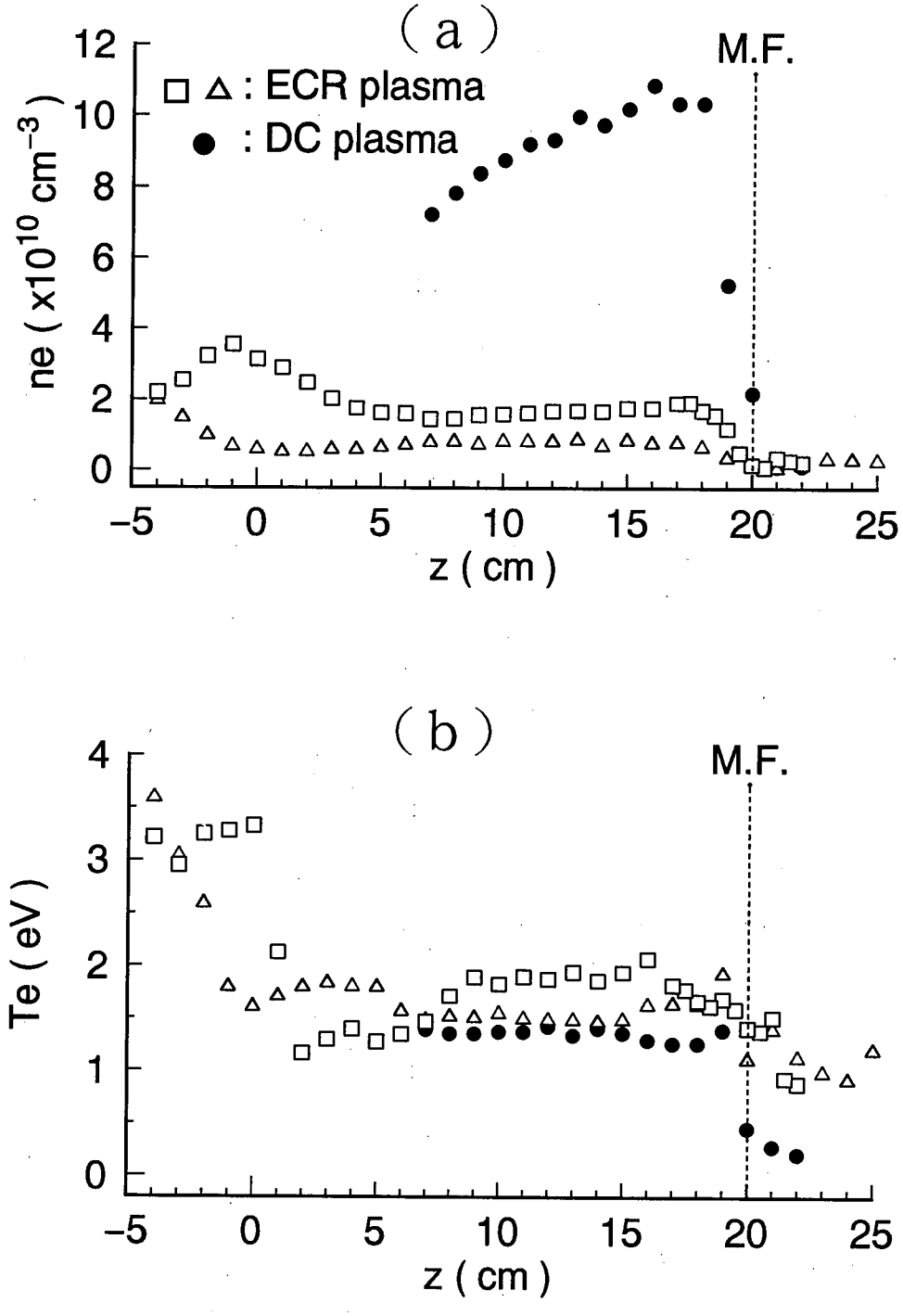
(a)
M.F.
□ △ : ECR plasma
● : DC plasma
ne (x10^10 cm^-3)
12
10
8
6
4
2
0
−5
0
5
10
15
20
25
z (cm)
(b)
M.F.
Te (eV)
4
3
2
1
0
−5
0
5
10
15
20
25
z (cm)

Fig.6

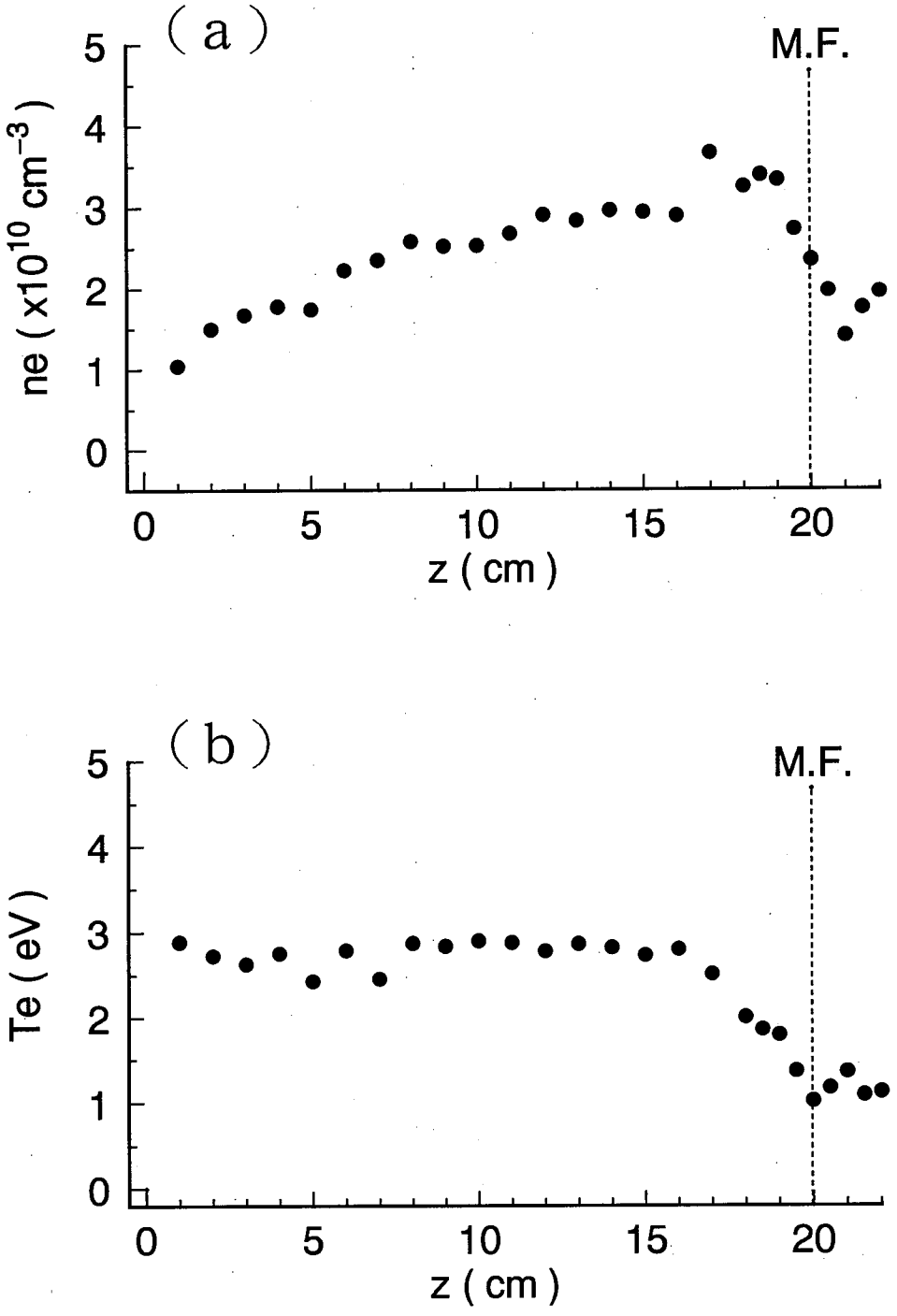
(a)
M.F.
ne (x10^10 cm^-3)
0
1
2
3
4
5
0
5
10
15
20
z (cm)
(b)
M.F.
Te (eV)
0
1
2
3
4
5
0
5
10
15
20
z (cm)

Fig.7

(a)

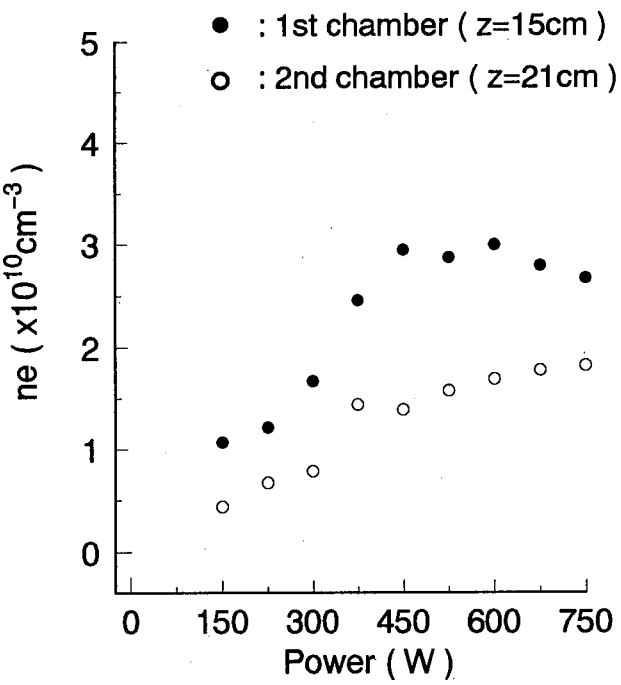
● : 1st chamber (z=15cm)
o : 2nd chamber (z=21cm)
ne (x10^10cm^-3)
0
1
2
3
4
5
0
150
300
450
600
750
Power (W)

(b)

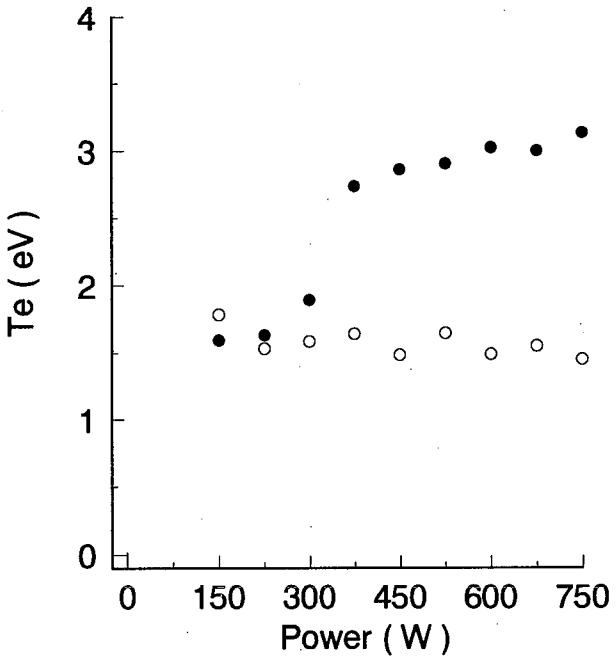
Te (eV)
0
1
2
3
4
0
150
300
450
600
750
Power (W)

Fig.8

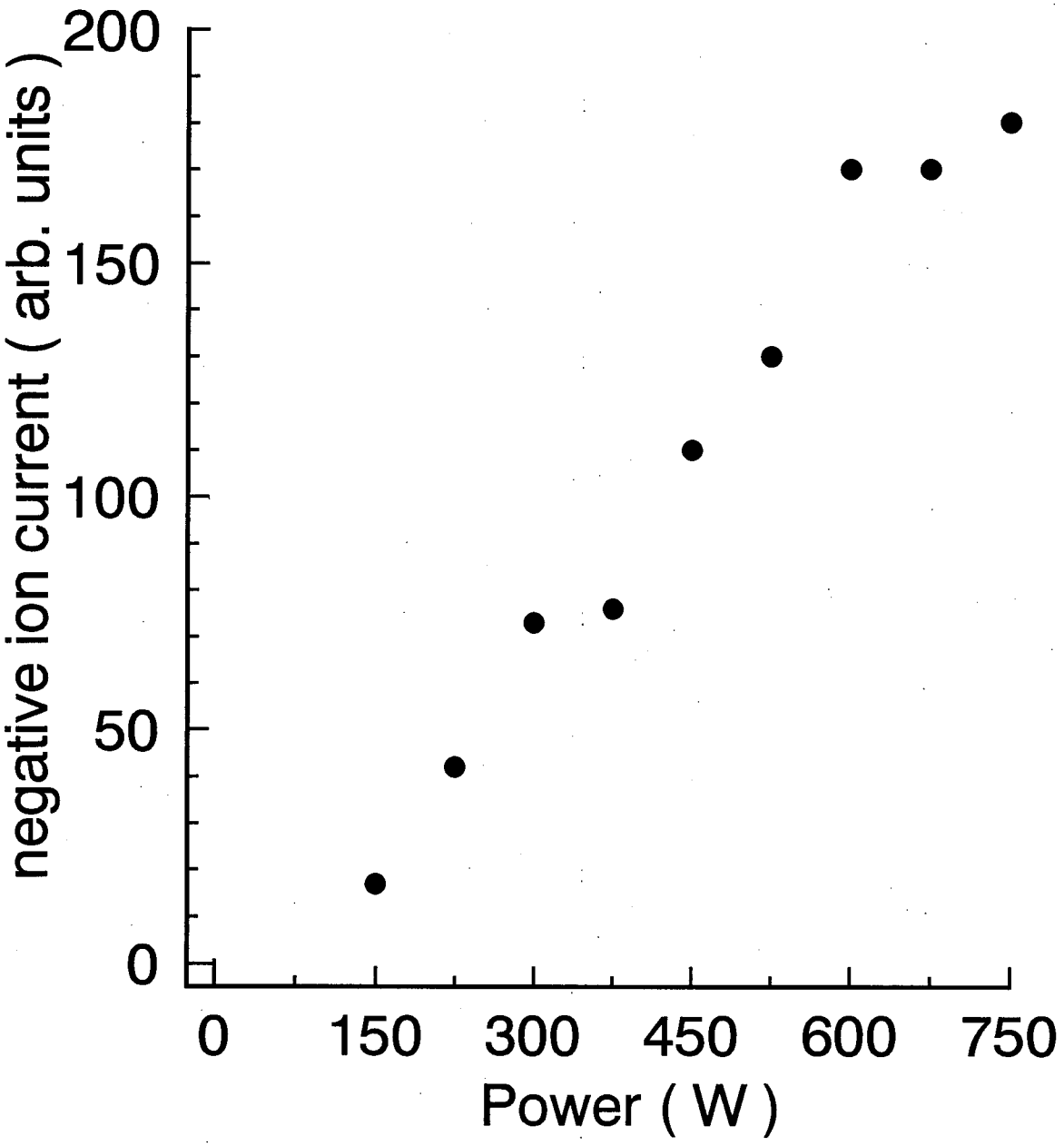
200
150
100
50
0
negative ion current (arb. units)
0
150
300
450
600
750
Power (W)

Fig.9